Gastroenterology 2020;158:1682–1697

Identification of Subtypes of Barrett's Esophagus and Esophageal Adenocarcinoma Based on DNA Methylation Profiles and Integration of Transcriptome and Genome Data

SriGanesh Jammula,[1,*] **Annalise C. Katz-Summercorn**,[2,*] **Xiaodun Li**,[2,*] Constanza Linossi,[2] Elizabeth Smyth,[2] Sarah Killcoyne,[2,3] Daniele Biasci,[1] Vinod V. Subash,[2] Sujath Abbas,[2] Adrienn Blasko,[2] Ginny Devonshire,[1] Amber Grantham,[2] Filip Wronowski,[2] Maria O'Donovan,[4] Nicola Grehan,[2] Matthew D. Eldridge,[1] Simon Tavaré,[1,5] the Oesophageal Cancer Clinical and Molecular Stratification (OCCAMS) consortium, Rebecca C. Fitzgerald[2]

[1]Cancer Research UK, Cambridge Institute, University of Cambridge, Cambridge, United Kingdom; [2]MRC Cancer Unit, Hutchison/MRC Research Centre, University of Cambridge, Cambridge, United Kingdom; [3]European Molecular Biology Laboratory, European Bioinformatics Institute (EMBL-EBI), Hinxton, United Kingdom; [4]Department of Histopathology, Cambridge University Hospital NHS Trust, Cambridge, United Kingdom; [5]Irving Institute for Cancer Dynamics, Columbia University, New York, New York.

See Covering the Cover synopsis on page 1516.

BACKGROUND & AIMS: Esophageal adenocarcinomas (EACs) are heterogeneous and often preceded by Barrett's esophagus (BE). Many genomic changes have been associated with development of BE and EAC, but little is known about epigenetic alterations. We performed epigenetic analyses of BE and EAC tissues and combined these data with transcriptome and genomic data to identify mechanisms that control gene expression and genome integrity. **METHODS:** In a retrospective cohort study, we collected tissue samples and clinical data from 150 BE and 285 EAC cases from the Oesophageal Cancer Classification and Molecular Stratification consortium in the United Kingdom. We analyzed methylation profiles of all BE and EAC tissues and assigned them to subgroups using non-negative matrix factorization with k-means clustering. Data from whole-genome sequencing and transcriptome studies were then incorporated; we performed integrative methylation and RNA-sequencing analyses to identify genes that were suppressed with increased methylation in promoter regions. Levels of different immune cell types were computed using single-sample gene set enrichment methods. We derived 8 organoids from 8 EAC tissues and tested their sensitivity to different drugs. **RESULTS:** BE and EAC samples shared genome-wide methylation features, compared with normal tissues (esophageal, gastric, and duodenum; controls) from the same patients and grouped into 4 subtypes. Subtype 1 was characterized by DNA hypermethylation with a high mutation burden and multiple mutations in genes in cell cycle and receptor tyrosine signaling pathways. Subtype 2 was characterized by a gene expression pattern associated with metabolic processes (ATP synthesis and fatty acid oxidation) and lack methylation at specific binding sites for transcription factors; 83% of samples of this subtype were BE and 17% were EAC. The third subtype did not have changes in methylation pattern, compared with control tissue, but had a gene expression pattern that indicated immune cell infiltration; this tumor type was associated with the shortest time of patient survival. The fourth subtype was characterized by DNA hypomethylation associated with structure rearrangements, copy number alterations, with preferential amplification of *CCNE1* (cells with this gene amplification have been reported to be sensitive to CDK2 inhibitors). Organoids with reduced levels of *MGMT* and *CHFR* expression were sensitive to temozolomide and taxane drugs. **CONCLUSIONS:** In a comprehensive integrated analysis of methylation, transcriptome, and genome profiles of more than 400 BE and EAC tissues, along with clinical data, we identified 4 subtypes that were associated with patient outcomes and potential responses to therapy.

Keywords: prognostic factor; antitumor immune response; response to treatment; gene repression.

Esophageal cancer is the eighth most common cancer type globally.[1] Esophageal adenocarcinoma (EAC) is the predominant subtype in the western world, particularly among white men[2]; most patients present at an advanced stage and despite some improvements in therapy, overall 5-year survival rate is less than 15%.[3] Epidemiologically, long-term esophageal exposure to acid and bile reflux appear to be the major risk factors resulting in aberrant differentiation of the cells lining the lower esophagus to intestinal metaplasia, otherwise known as Barrett's esophagus[4] (BE).

Recent genomic studies have shown that BE harbors a number of point mutations even in cases that never progress to cancer[5]; however, it has a relatively stable genome in terms of copy number alterations and structural variants

***Authors share co-first authorship.**

Abbreviations: **BE, Barrett's esophagus; CAF, cancer-associated fibroblast; CpGi, CpG island; CIMP, CpG island methylator phenotype; EAC, esophageal adenocarcinoma; GZMB, granzyme B; NMF, non-negative matrix factorization; RNA-seq, RNA-sequencing; SV, structural variant; TCGA, The Cancer Genome Atlas; WGS, whole-genome sequencing.**

Most current article

0016-5085/$36.00
https://doi.org/10.1053/j.gastro.2020.01.044

WHAT YOU NEED TO KNOW

BACKGROUND AND CONTEXT

Esophageal adenocarcinomas (EAC) are heterogeneous and often preceded by Barrett's esophagus (BE). There is information on transcriptomes and genomes of these tissues, but these data have not been integrated with epigenome data.

NEW FINDINGS

In an integrated epigenome, genome, and transcriptome analysis of methylation patterns of more than 400 BE and EAC tissue samples, the authors identified 4 subtypes, associated with patient outcomes and potential responses to therapy.

LIMITATIONS

This was a retrospective analysis of tissue samples and patient data. Prospective studies are needed.

IMPACT

Analyses of genome, transcriptome, and epigenome features of BE and EAC samples could increase our understanding of pathways of development and identify therapeutic targets and prognostic factors.

(SVs).[6,7] As BE progresses to EAC, there is loss of p53 accompanied by an increasingly unstable genome, although the genetic trigger for disease progression has not been established.[5,8] DNA methylation is one of the key epigenetic mechanisms for regulating gene expression and maintaining genome stability.[9] In a number of different cancer types, it has been shown that hypermethylation at CpG islands (CpGi), including promoter regions, results in gene silencing of tumor suppressor genes, whereas regions undergoing hypomethylation are associated with increased expression of oncogenes and genome instability.[10]

In EAC, 2 studies have demonstrated marked variation in the degree of methylation at CpGi, denoted CpGi methylator phenotype (CIMP)-positive and -negative respectively.[11,12] The Cancer Genome Atlas (TCGA) study has shown that methylation profiles of esophageal squamous cell carcinoma and EAC are distinct, and the methylation profile of EAC resembles that of intestinal cancers, such as gastric and colon cancer.[13] However, the detailed landscape of methylation changes across BE and EAC in relation to other genome-wide mutational processes determined from whole-genome sequencing (WGS) data remains to be determined.

Here we present methylation data integrated with genomic and transcriptomic information for a large cohort comprising more than 400 cases. The detailed clinical information has enabled us to examine the prognostic significance of the changes and we have used primary organoid models to test the therapeutic relevance of prevalent epigenetically regulated targets.

Methods

Cohort

In this retrospective cohort study, we assessed 150 BE and 285 EAC cases derived from the Biomarker and International Cancer Genome Consortium study, for which samples are collected through the UK-wide OCCAMS (Oesophageal Cancer Classification and Molecular Stratification) consortium. The procedures for obtaining the samples, quality control processes, extractions, and WGS are as previously described.[6] Strict pathology consensus review was observed for these samples with a 70% cellularity requirement before inclusion.

Methylation Profiling and Data Analysis

Methylation profiles for all samples were generated using the EPIC array platform. For all samples, DNA from fresh frozen material was used. All raw data were processed using minfi.[14] Samples with less than 96% capture efficiency were not considered in analysis. We filtered probes if they were not significantly detected from background, and are not in CpG context, have known single nucleotide polymorphisms in the surrounding locus, align to multiple locations in the genome, or if they mapped to X and Y chromosomes. Processed methylation data were further normalized using BETA mixture model BMIQ[15] implemented in ChAMP package.[16] Processed data were then corrected for batch effects using limma.[17]

To identify methylation-dependent subgroups, we performed non-negative matrix factorization (NMF)[18] on 5000 most variable probes together with k-means clustering. Through NMF we first estimated optimal ranks/metagenes by executing it in combinations of 2 to 10 metagenes over 200 runs. This analysis identified 4 optimal metagenes assessed through the cophenetic index. Scores from all 4 metagenes were further subjected to k-means clustering for identifying the optimal number of subtypes. Using silhouette width as a measure, 4 optimal subtypes were identified.

Differential analysis on individual probes was performed using linear models implemented in limma.[17] We selected as differentially methylated only those probes with an absolute difference in β greater than 0.3 and adjusted P value less than .01. On the other hand, for identifying regions with differential methylation, we used the bumphunter[19] function implemented in minfi. bumphunter was executed under the following parameter settings: maxGap = 500, B = 1000, cutoff = 0.2, and minProbes = 4.

WGS Data Analysis

WGS data were aligned using BWA-MEM program. We used Strelka[20] for calling somatic mutations, ASCAT[21] for calling copy number, and Manta[22] for calling SVs under similar settings, as previously described.[6] Our methods were benchmarked against various other available methods and have among the best sensitivity and specificity for variant calling (International Cancer Genome Consortium benchmarking exercise[23]).

RNA-sequencing Data Analysis

Sequencing data were aligned using STAR aligner.[24] Using ENSEMBL gene annotation, counts of individual genes for all samples were computed using GenomicAlignments[25] package from Bioconductor. Based on the counts, sequencing depth of individual samples, and gene annotation, Transcripts Per Kilobase Million (TPM) for individual genes was computed across all samples. TPM was further corrected for batch effects using Combat.[26]

Differential analysis of each individual subtype over all other subtypes was performed on counts using the edgeR[27]

package. Pathway analysis was performed on ranked data from differential analysis using Gene Set Enrichment Analysis.[28] For such analyses, we considered pathways annotated from Gene Ontology, Reactome and other databases.

Enrichment for different immune cell types was computed through gene set variant analysis.[29] Markers for immune cell types were retrieved from publication.[30]

Identifying Epigenetically Silenced Genes

For assessing which genes undergo transcriptional repression under the influence of gaining methylation in promoter regions, we performed integrative methylation and RNA-sequencing (RNA-seq) analysis. For this analysis, we considered samples for which both RNA-seq and methylation were available. For each gene, we identified all probes located 1500 base pairs both up and downstream from the transcription start site. We selectively removed all CpG sites that were methylated in normal tissues (mean β-value >0.2). Methylation data was then dichotomized using β-value ≥ 0.3 as a threshold (as used in TCGA studies[13,31]) for positive DNA methylation, and discarded CpG sites methylated in fewer than 10% of samples. For each probe/gene pair, we then applied the following conditions: (1) categorized samples as either methylated ($\beta \geq 0.3$) or unmethylated ($\beta < 0.3$); (2) compare expression in the methylated and unmethylated groups using the Mann-Whitney test; and (3) compute the correlation between methylation beta and expression TPM. We labeled each individual tumor sample as epigenetically silenced for a specific probe/gene pair selected previously if for the probes there is a difference in beta (>0.2) between 2 groups, difference in distribution of expression of (adjusted $P < .05$), and negative correlation between methylation and expression ($r < -0.1$, adjusted $P < .05$). Only genes with multiple probes were considered for this analysis and a sample is considered as epigenetically silenced if more than 30% of probes for the corresponding gene was also labeled as epigenetically silenced.

Transcription Factor Analysis

We used ELMER[32] for understanding which transcription factors are regulated on perturbations from regulatory regions. Briefly, this method is based on initially identifying differentially methylated distal probes and predicting enriched motifs across them. Methylation levels from motif-associated probes are then correlated with expression levels of transcription factor and ranked for any significant associations. We performed supervised analysis where each subtype was compared with others. On doing so, we did not find significant results for most of the comparisons except for one, that between Subtype 2 and Subtype 3.

Ethics

The study was registered (UKCRNID 8880), approved by the Institutional Ethics Committees (REC 07/H0305/52 and 10/H0305/1), and all subjects gave individual informed consent.

Data Availability

Methylation data is accessible from European Genome-phenome Archive under accession numbers EGAD00010001822, EGAD00010001838 and EGAD00010001834.

Results

To capture comprehensive genome-wide methylation changes, we used the Illumina MethylationEPIC BeadChip (EPIC; Illumina Inc., San Diego, CA). EPIC measures methylation over 850,000 CpG sites covering a wide range of regulatory regions of the genome (https://emea.illumina.com/products/by-type/microarray-kits/infinium-methylation-epic.html). Compared with its older version Illumina HumanMethylation450 BeadChip (450K; Illumina Inc.), more than 90% of 450K probes are included in EPIC along with increased coverage over distal regulatory elements.[33] In total, 435 samples comprising 285 EAC and 150 BE cases along with 100 controls were assayed using the EPIC array. We included control samples from neighboring tissue types: squamous esophagus (n = 39) and gastric cardia (n = 38), as well as duodenum (n = 23) as a comparison for intestinal differentiation, which is a defining feature of BE and also seen in well-differentiated EAC. Both methylation and RNA-seq–specific analysis among the 3 control tissue types showed that each tissue harbors a unique pattern of methylation (Supplementary Figure 1*J*) and RNA expression (Supplementary Figure 1*K*). The gene ontology of differentially expressed genes shows enrichment of pathways specific to each individual tissue (Supplementary Figure 1*L*). As expected, biological processes related to epidermis development and keratin differentiation are specifically enriched in squamous tissue. Similarly, in gastric tissue we observe upregulation of hormone and gastric acid secretion processes, whereas lipid-associated metabolic processes are enriched in duodenum. Biological processes such as digestion and ion transport are enriched in both gastric and duodenum tissues, in keeping with some common functional roles. For 59% of BE cases and 62% of EAC cases, both WGS, and transcriptomic (RNA-seq) data were available to enable an integrated analysis (Supplementary Figure 1*A* and *B*).

The clinical features of the cohort generated from the UK-wide OCCAMS consortium are in keeping with the expected demographics for this disease (Supplementary Tables 1 and 2). Most cases are male (85% EAC, 83% BE) with a median age of 67 years. The most common site of EAC cases is at the gastro-esophageal junction and most patients included are stage 2 or 3 (89%), in keeping with our recruitment in the context of patients entering a curative pathway for whom sample collection is most feasible. Among the premalignant BE cases, 57% are nondysplastic and the remaining 43% are dysplastic. Most of these are taken from patients undergoing surveillance and represent their highest progression grade following multiple years of follow-up. We also included 34 cases with BE adjacent to invasive EAC (see Supplementary Table 2 and Supplementary Figure 2*C*–*E* for details).

Methylation Profiles of BE and EAC Reveal 4 Subtypes With Independent Replication

To elucidate differences between BE and EAC in comparison with controls, we carried out principal component analysis on the 5000 most variable probes selected across all samples. It is apparent that, in keeping with their

glandular phenotype, BE and EAC closely resemble gastric cardia and duodenum but are highly distinct from normal squamous esophagus (Supplementary Figure 1*C*). Heterogeneous BE profiles overlap more strongly with EAC than with benign gastric and duodenal tissues.

In view of the variability in methylation observed in BE and EAC (Supplementary Figure 1*C*) we used NMF-based clustering to identify subtypes. Through this analysis, we were able to identify 4 optimal metagenes (Supplementary Figure 1*D*). Expression measures of these 4 metagenes were further subjected to k-means clustering, which resulted in 4 stable subtypes (Supplementary Figure 1*E* and *F*). Figure 1*A* represents levels of methylation across 5000 most variables with samples grouped into 4 identified subtypes. For comparative purposes, levels of methylation from different control samples are also displayed on the left. Interestingly, the BE cases are distributed across the 4 subgroups: 83.2% of the cases in subtype 2 are BE (n = 119; BE = 99, EAC = 20) with 33.3% (n = 99; BE = 33, EAC = 66) in subtype 3, 13.6% in subtype 1 (n = 125; BE = 17, EAC = 108) and a single case in subtype 4 (n = 92; BE = 1, EAC = 91) (Figure 1).

From the heatmap (Figure 1*A*), we can observe that each subtype has a unique methylation pattern; 30.6% of the variable probes are localized within CpGi with the remainder falling in areas designated as shore (2 kb outside CpGi boundaries), shelf (2 kb outside shore), and open sea. Similarly, in gene centric terms, 42.7% of the most variable probes are localized in promoter regions. For ease of reference, we have divided probes into 3 blocks: A, B, and C. In block A, most probes overlap with CpGi (orange) and are located in promoter regions (blue), whereas most probes in block B and C fall within gene bodies and intergenic regions. There is generally a gain in methylation for block A probes in subtypes 1 and 2 when compared with that of controls and the other subgroups. In contrast, probes in block B are relatively hypomethylated in subtype 4 and probes from block C are unmethylated in subtype 2. For EACs, except for differentiation status, we did not find any significant association between subtypes and clinical variables, such as tumor location, chemotherapy status, differentiation status (Supplementary Figure 2*A* and *B*). The distribution of BE cases is influenced by the degree of dysplasia, with most of the nondysplastic BE falling into subtypes 2 and 3 (Supplementary Figure 2*C*–*E*). From here onward in some figures, subtype 1 is denoted as ST_1, subtype 2 as ST_2, subtype 3 as ST_3, and subtype 4 as ST_4.

To determine whether these subtypes are specific to this cohort or a result of the methodology used, we examined whether these findings could be replicated in an independent cohort. To do this, we examined publicly available methylation data from Australia, comprising 19 BE and 125 EAC cases along with 106 controls (normal esophagus and gastric) profiled using the older 450K array platform.[11] Remarkably, although the probe overlap between the 2 platforms was only 55.4% (2771 of the 5000 most variable probes), we observed a similar number of metagenes and again 4 subtypes emerged with very similar methylation profiles to those seen in our cohort (Supplementary Figure 2*F*–*H*).

Methylation Profiles in Relation to DNA Mutation

When integrating the WGS data, which were available for most cases (n = 391/435), Subtype 1 and 4 are observed to have a significantly higher mutation burden compared with subtypes 2 and 3 (Supplementary Figure 1*H*). The low mutation burden in Subtype 2 is partly explained by the high proportion of premalignant BE cases, but the difference persists in EAC cases.[5,8]

We previously identified 77 genes that, based on their "driver gene" status, are likely to play a critical role in the pathogenesis of EAC.[7] We mapped the 20 driver genes mutated in at least 4% of EAC cases (Figure 1*B*, Supplementary Figure 3). TP53 and CDKN2A are the 2 most frequently altered genes across the cohort as expected,[7] wherein TP53 is more preferentially mutated in subtype 1 (78%) and subtype 4 (78%), whereas in Subtype 2 and subtype 3, 37% and 46%, are altered. Similarly, CDKN2A is preferentially deleted in subtype 2, commensurate with the high prevalence of BE (67%, $P < .001$). ERBB2 is amplified in both subtype 1 (19%) and subtype 4 (29%). Some genetic events appear to be subtype specific; for example, GATA4 (22%, $P < .001$), CCND1 (21%, $P < .001$), KCNQ3 (19%, $P = 0.01$), MYC (23%, $P < .01$), CDK6 (17%, $P < .05$), and KRAS (18%, $P < .05$) are preferentially altered in subtype 1, whereas CCNE1 (21%, $P < .001$) and APC (12%, $P < .05$) are preferentially altered in subtype 4. Mapping these events to their functional pathways, we found that components of the receptor tyrosine kinase pathway (GATA4, ERBB2, KRAS) and cell cycle (CCND1, CCNE1, MYC, CDK6) are altered in subtypes 1 and 4. More specifically, all key drivers of cell cycle aside from CCNE1 are preferentially altered in subtype 1, whereas components of the Wnt pathway (APC) are dysregulated in subtype 4. MDM2 is amplified preferentially in subtype 3 (8%, $P = .0643$).

Integrated Analysis of Methylation, Genomic and Expression Features in Each Subgroup

Subtype 1. To characterize the highly mutated subtype 1 in more detail, we performed a differential analysis in comparison with the controls both at an individual base level and to broad regions for which probes clustered within a distance of 500 base pairs. We found that the proportion of hyper- and hypomethylated probes was similar. However, hypomethylation events are spread throughout the genome, whereas hypermethylation is profound in localized regions, mainly promoters rich with CpGi (Figure 2*A*). Further, we observed that 66% of hypermethylated probes and 1% hypomethylated probes overlap with CpGi and most (59%) occur in promoter regions (Figure 2*B*), suggesting a CIMP-like phenotype.

Because the state of chromatin can further affect gene regulation, we explored markers of closed and open chromatin. To do this, we took advantage of Histone modification data available from ENCODE[34,35] and the ROADMAP epigenomics consortium.[36] Using methylation profiles, we

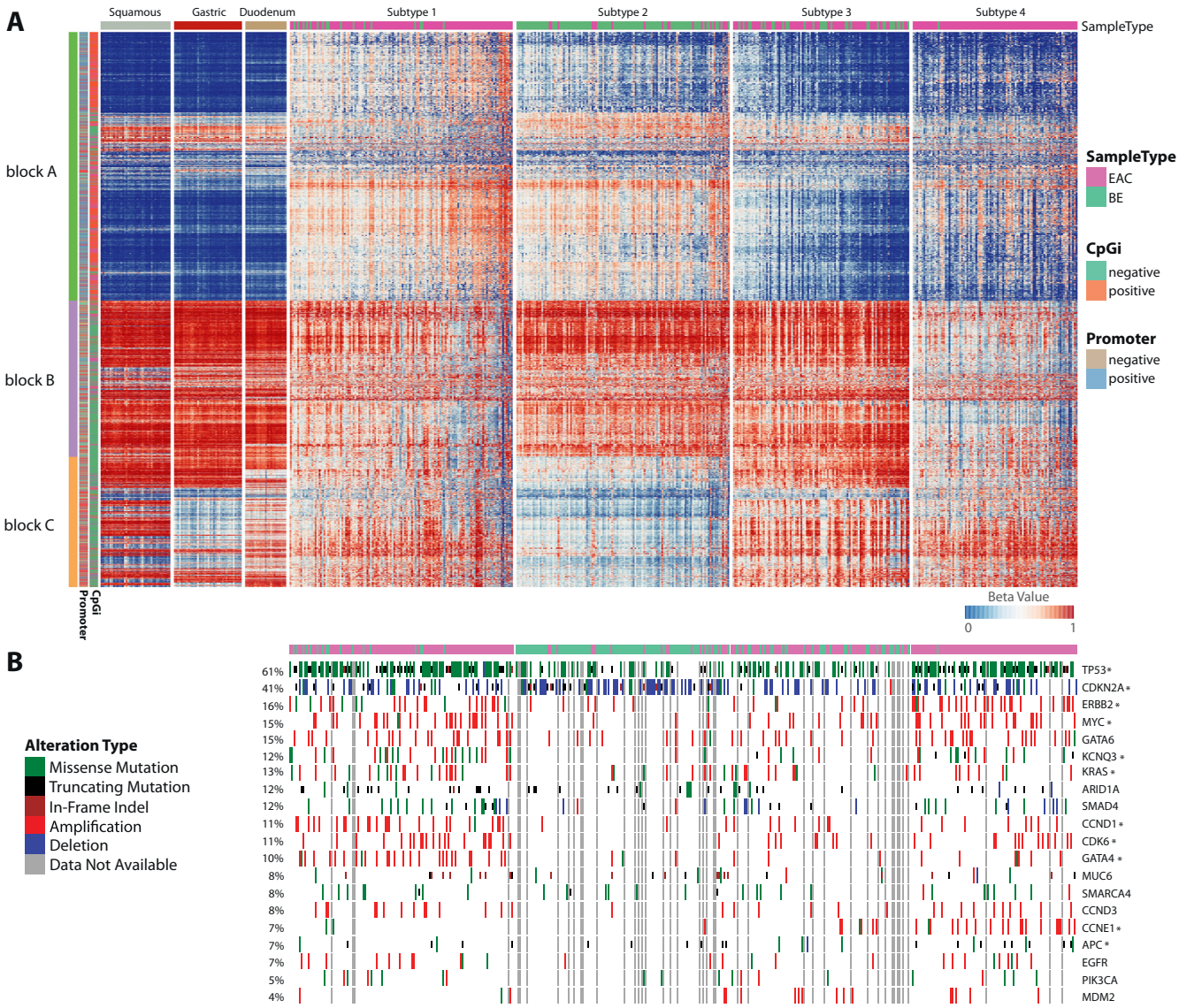

Figure 1. Methylation-based BE/EAC subtypes. (*A*) Heatmap representing methylation levels from top 5000 most variable CpGs across all cases categorized into 4 subtypes: subtypes 1, 2, 3, and 4, including 3 different controls (squamous, gastric, duodenum) in extreme left along with annotation of CpG with different color code. (*B*) Mutation status of driver genes across all cases in same order as displayed in (*A*).

confirmed tissue-specific similarity for healthy controls between ENCODE and our dataset (Supplementary Figure 1*M* and *N*). We then compared both repressive Histone 3 methylation at Lysine 27 (H327me3) and activation marks with Histone 3 acetylation at Lysine 27 (H3K27ac) data from squamous, gastric, and duodenum tissues available from the ENCODE[34,35] and ROADMAP epigenomics consortium.[36] This showed that for hypermethylation, 77% of regions are marked by H3K27me3 and 23% by H3K27ac (Figure 2*C*) across all tissues. Hence, the effects of DNA methylation on gene regulation do not appear to be tissue specific.

Transcriptome-based pathway analysis of subtype 1 in comparison with all other subtypes shows a strong enrichment for pathways related to DNA repair and cell cycle (Figure 2*D*, Supplementary Table 6), which is also in line with driver gene alterations (CCND1, CCNE1, MYC, CDK6) described previously.

Subtype 2. Subtype 2 is dominated by BE cases with hypermethylated CpGi. We were interested to assess whether the hypermethylation changes in this subtype are also seen in EAC, so we compared differentially hypermethylated probes in subtypes 1 and 2. This showed that most (85%) hypermethylated probes are shared between these subtypes for BE and EAC, suggesting that hypermethylation is an early event (Figure 1*A* and *B*).

Even though we observe strong similarities in hypermethylation patterns between BE and EAC, there is also a prominent pattern of unmethylated block C probes (Figure 1*A*) that are highly specific to BE cases in this subgroup. We suspect that these are unique regions that maintain tissue specificity in BE and in keeping with this,

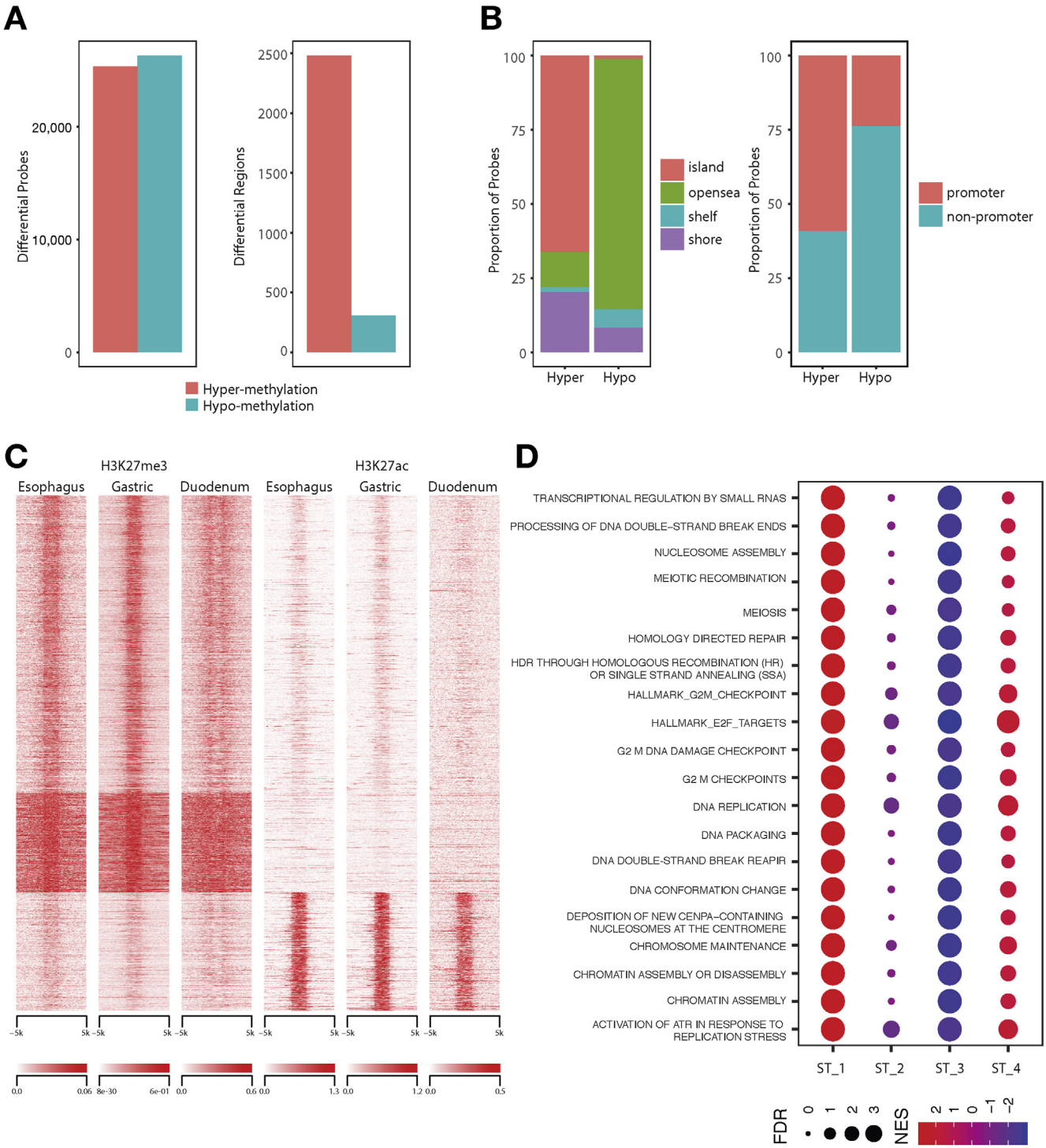

Figure 2. Hypermethylation-driven subtype 1. (*A*) Total number of hyper- and hypomethylation events observed in subtype 1 at individual CpG base level (*left*) and regions with clustered probes (*right*). (*B*) Annotation of both of hyper- and hypomethylation events with respect to CpG island (*left*) and gene promoter (*right*). (*C*) Heatmap quantifying levels of H3K27me3 and H3K27ac in all extend regions undergoing hypermethylation. (*D*) Dot plot with top scored pathways identified in subtype 1 when compared with other subtypes through gene set enrichment analysis.

the levels are comparable with gastric but not with squamous or duodenum phenotypes (Figure 3*C*). It has been observed through functional studies that different sets of key master transcription factors, such as ELF3, GATA6, KLF5, and TP63, through their self-regulatory networks can play an important role in esophageal cancer progression.[37,38] To predict the behavior of different transcription factors, we took advantage of distal probes and observed that key transcription factor motifs, including HNF4A/G, FOXA1/2/3, GATA6, and CDX2, are significantly

overrepresented in probes specific to distal regulatory regions in subtype 2 (Figure 3*D*). Correlation between the average DNA methylation levels at probes enriched for individual transcription factors and the relevant expression level across all subtypes is shown in Supplementary Figure 4. This demonstrates that the probes critical for regulation of master transcription factors to maintain the BE phenotype are unmethylated in subtype 2 with a gain in methylation at these sites and reduced expression in EAC. At the RNA level, there is selective enrichment of ATP synthesis, fatty acid metabolism, and oxidation-related processes in this subtype, especially in BE (Supplementary Figure 5*A*, Supplementary Table 7).

Subtype 3. Compared with other subtypes, we did not observe strong changes in methylation in subtype 3 however, from RNA-seq data, we observe that subtype 3 has a strong enrichment of both innate and adaptive immune cell types. Particularly, we notice strong positive enrichment of cytotoxic cells, B cells, mast cells, and neutrophils along with cancer-associated fibroblasts (CAFs) and at the same time we also observe reduced levels of T-helper cells in this subtype (Figure 4*A*). This contrasts with subtype 2, which shows no enrichment for immune infiltration (Figure 4*A*). Consistent with this, we observe that all pathways related to immune regulation are strongly enriched (Figure 4*B*, Supplementary Figure 5*B*, Supplementary Table 8). Granzyme B (GZMB), a serine protease protein secreted by cytotoxic and natural killer cells, is well known for its vital role in immune defense mechanisms. Using GZMB as marker of cytotoxic cells, we verified their abundance in multiple cases from different subtypes through immunohistochemical (IHC) staining and confirmed that the relative abundance of GZMB is substantially higher in subtype 3 as compared with other subtypes (Figure 4*C*, Supplementary Figure 5*D*).

The high level of immune infiltration in subtype 3 also suggests a proportionally lower tumor content (see Supplementary Figure 1*G*), as computationally predicted from WGS data. To ensure that cellularity is not influencing our subtype classification, we repeated NMF-based clustering on samples with computationally predicted cellularity greater than 0.3. On doing so, we still retain similar subtypes, suggesting cellularity has no impact on classification.

Subtype 4. Subtype 4 is dominated by hypomethylation events (Figure 5*A*), which in other studies may be an indication of genome instability.[39] Widespread hypomethylation has been observed in both early and late stages of many cancer types,[40–44] including BE and EAC,[45,46] causing upregulation of certain coding and noncoding regions. In our analysis, when compared with other subtypes, subtype 4 shows a relatively high number of copy number alterations, which are spread throughout the genome (Figure 5*B*). For example, focal amplifications of CCNE1, ERBB2, and Chr13 and 20 are common as compared with other subtypes. Subtype 4 also has more extrachromosomal-like events affecting ERBB2, characterized by more than 10 copies of the gene, whereas in subtype 1, most events are low-level amplifications (Figure 5*C*). This is consistent with our previous finding that these extrachromosomal-like events are strongly associated with chromosomal rearrangements.[7] When quantifying the total number of SVs, subtype 4 was found to have significantly more SVs as compared with other subtypes (Supplementary Figure 1*I*). On a case-by-case basis, patients in group 4 with low levels of methylation harbor a high level of SVs (Figure 5*D*), in keeping with the idea that methylation levels may be important for maintaining genome stability.

When considering the prognosis of EAC cases according to their methylation profiles (BE cases were removed for this analysis), there are differences in overall survival rates among the subgroups (Figure 5*E*). The small number of EAC cases in subtype 2, which cluster with the BE cases, had the best survival. Surprisingly, subtype 3, which has an immune activation phenotype, a lower mutation burden, and fewer oncogenic drivers, has poor survival compared with patients in other subtypes.

Epigenetically Silenced Genes and Relevance to Therapy

To understand which genes undergo transcriptional repression in association with methylation change, we performed an integrative methylation and transcriptomic analysis. Of the 237 genes with significantly lower expression in relation to increased methylation (Supplementary Table 3), few genes seem to be affected globally across all subtypes, with most silenced genes being more specific to subtypes 1 and 2 (Figure 6*A*).

Gene ontology and pathway analysis of silenced genes showed enrichment for biological processes related to transcription and its regulation, along with pathways related to cell cycle (CCND2, RDX, UBE2E2), kinase signaling, stem cell pluripotency, nucleosome assembly, cell adhesion, and wnt/β-catenin signaling pathway, which has been shown to play a role in the neoplastic transformation of BE[47] (Supplementary Figure 6*A* and *B*, Supplementary Tables 4 and 5). We also observe that a few immune regulators (BLNK, CD40, VAV3, IRS2) are also affected by methylation.

Previously we tested different sets of drugs in both EAC cell lines and primary derived organoids and have shown that their response correlates with the specific driver gene alterations.[7,48] In view of this, we were interested to identify methylation-based drivers and predict their response to known drugs. Previous work has shown that the MGMT gene, a key regulator in DNA repair, is methylated in nearly 50% of glioblastoma cases, and these patients benefited from temozolomide chemotherapy more than patients with an unmethylated MGMT promoter.[49] In our cohort, MGMT is strongly regulated by a gain of methylation in promoter regions, affecting 32% of cases (Figure 6*B*, Supplementary Figure 6*C*). To examine responses to temozolomide in EAC, we took advantage of organoids generated from primary tumors from this cohort.[48] High sensitivity to temozolomide was observed in organoids showing low

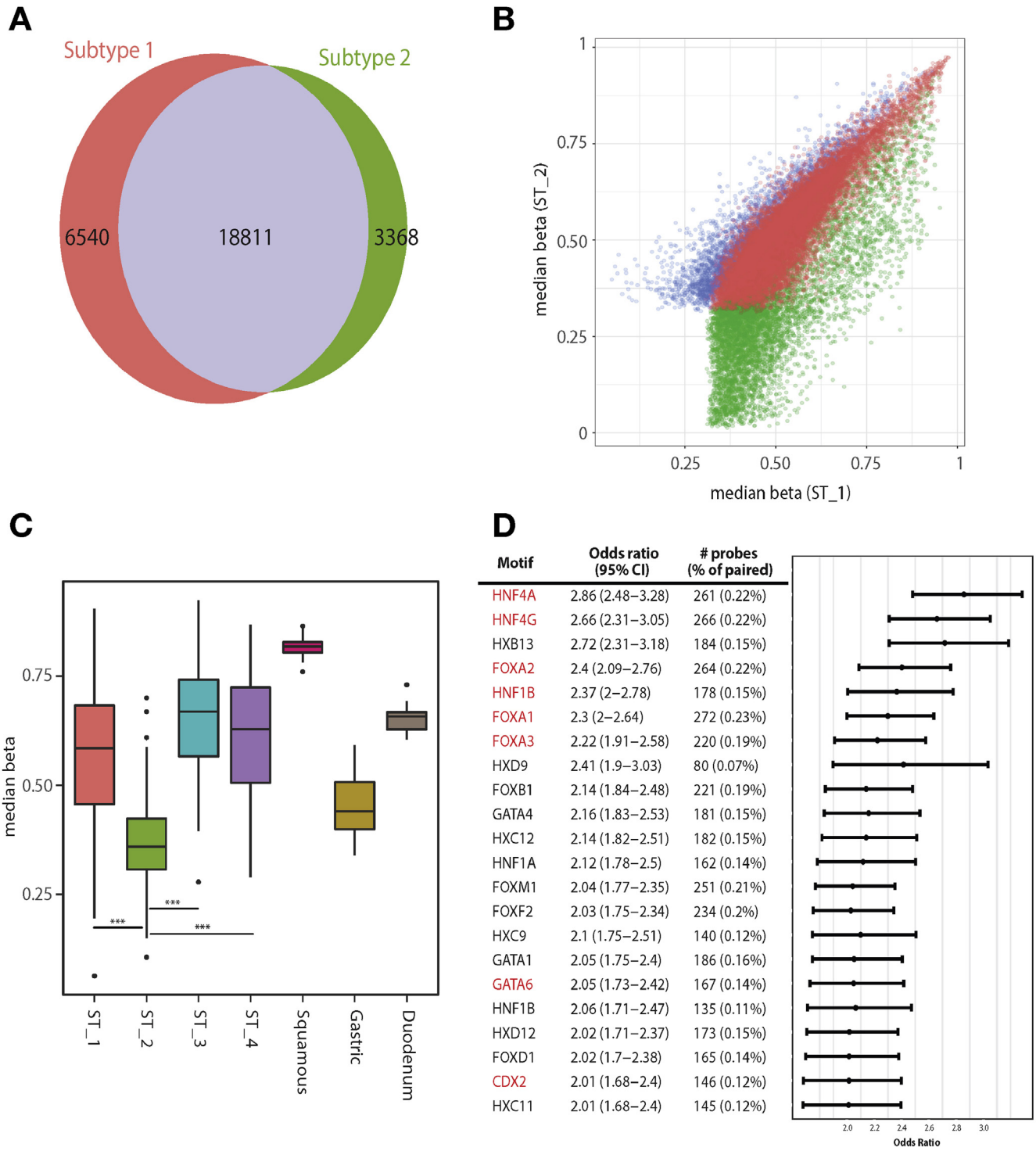

Figure 3. BE-specific subtype 2. (*A*) Venn diagram showing level of common probes undergoing hypermethylation between subtypes 1 and 2. (*B*) Correlation plot comparing median level of methylation from all probes undergoing hypermethylation in subtype 1 and 2. (*C*) Boxplot comparing median level of methylation across 4 different subtypes, including controls for all probes from block C from Figure 1*A* (*P* value: *< .05, **< .01, ***< .001). (*D*) Plot shows odds ratio with 95% confidence interval for set of transcription factors motifs enriched in subtype 2. Key transcription factors required for maintaining BE phenotypes are highlighted in *red*.

expression of MGMT at both RNA and protein levels, such as CAM277, in contrast, organoids with stable MGMT expression showing resistance, for example in CAM408 (Figure 6*D* and *E*, Supplementary Figure 6*E*).

Similarly, CHFR, a cell cycle check point inhibitor, is methylated in many cancer types; in squamous cell carcinoma, CHFR methylation sensitizes to taxane chemotherapy.[50] In our cohort, we observe CHFR to be altered in 18% of cases, most of

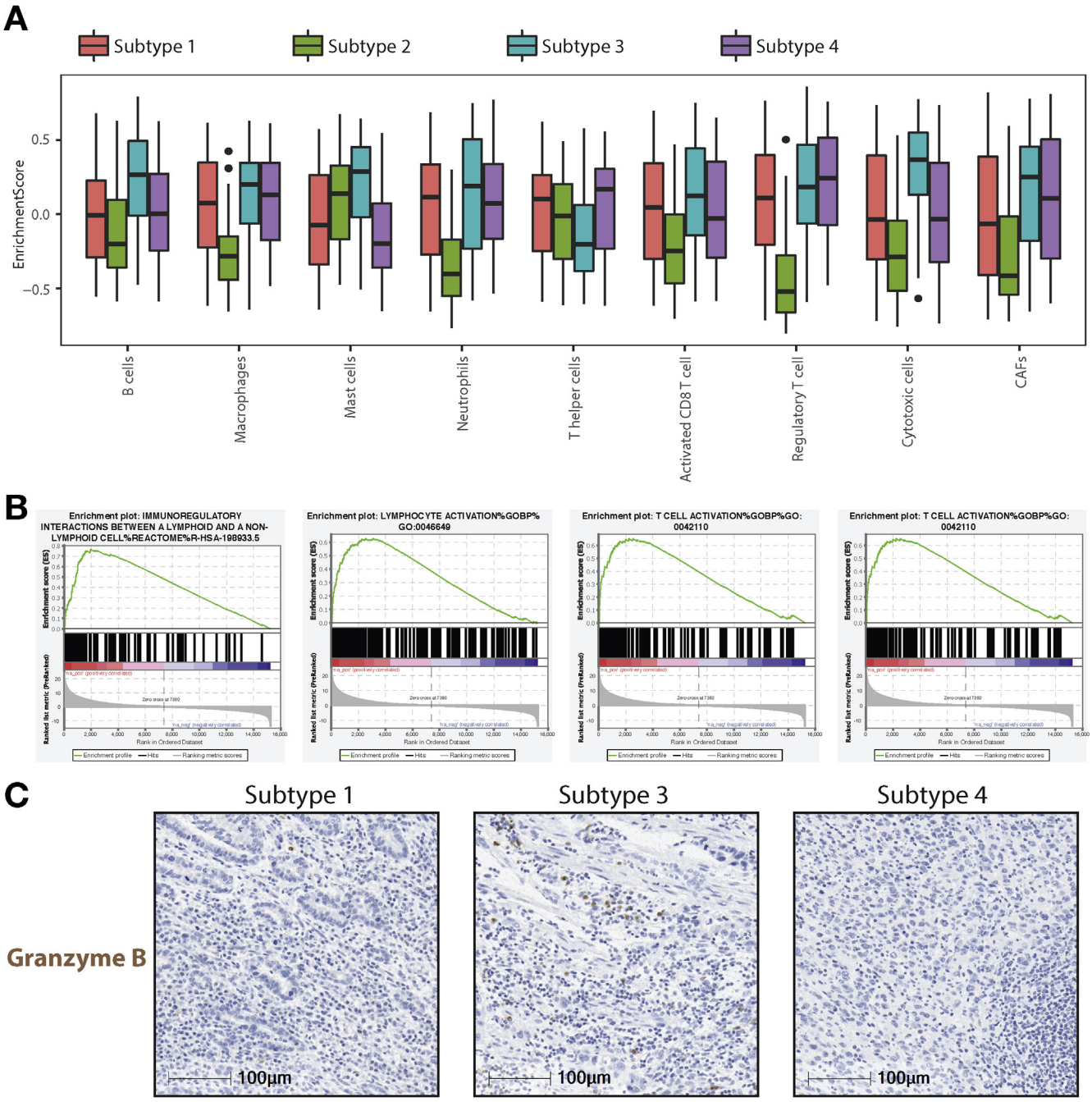

Figure 4. Immune-regulated subtype 3. (*A*) Boxplot displaying enrichment scores for different immune cell types computed from bulk RNA-seq data across all 4 different subtypes. (*B*) Gene set enrichment plot for key immune-regulated pathways identified on comparing subtype 3 with all other subtypes. (*C*) Immunohistochemistry staining for granzyme B on 3 different chemo-treated cases representative of subtype 1, 3, and 4.

which are preferentially affected in subtype 1 (Figure 6*C*, Supplementary Figure 6*D*), and in organoid models, CHFR expression levels correlate with a differential response to docetaxel (Supplementary Figure 6*D*).

In our earlier driver gene analysis, we have shown that more than 50% of EACs (n = 551) are predicted to benefit from CDK4/6 inhibitors, along with EZH2 and BET inhibitors in a smaller proportion of cases.[7] In view of this observation, we were interested to determine whether the response rate to different inhibitors is also dependent on their methylation profiles. We observe CDK4/6 inhibitors to be effective in EAC, across all subtypes. In contrast, we also observe CDK2 ($P < .001$) inhibitors to be more effective in subtype 4 (Figure 6*F*). This selective response is due to preferential amplification of CCNE1 in subtype 4.

Discussion

NMF-based clustering demonstrated that both BE and EAC can be broadly classified into 4 subtypes each with a

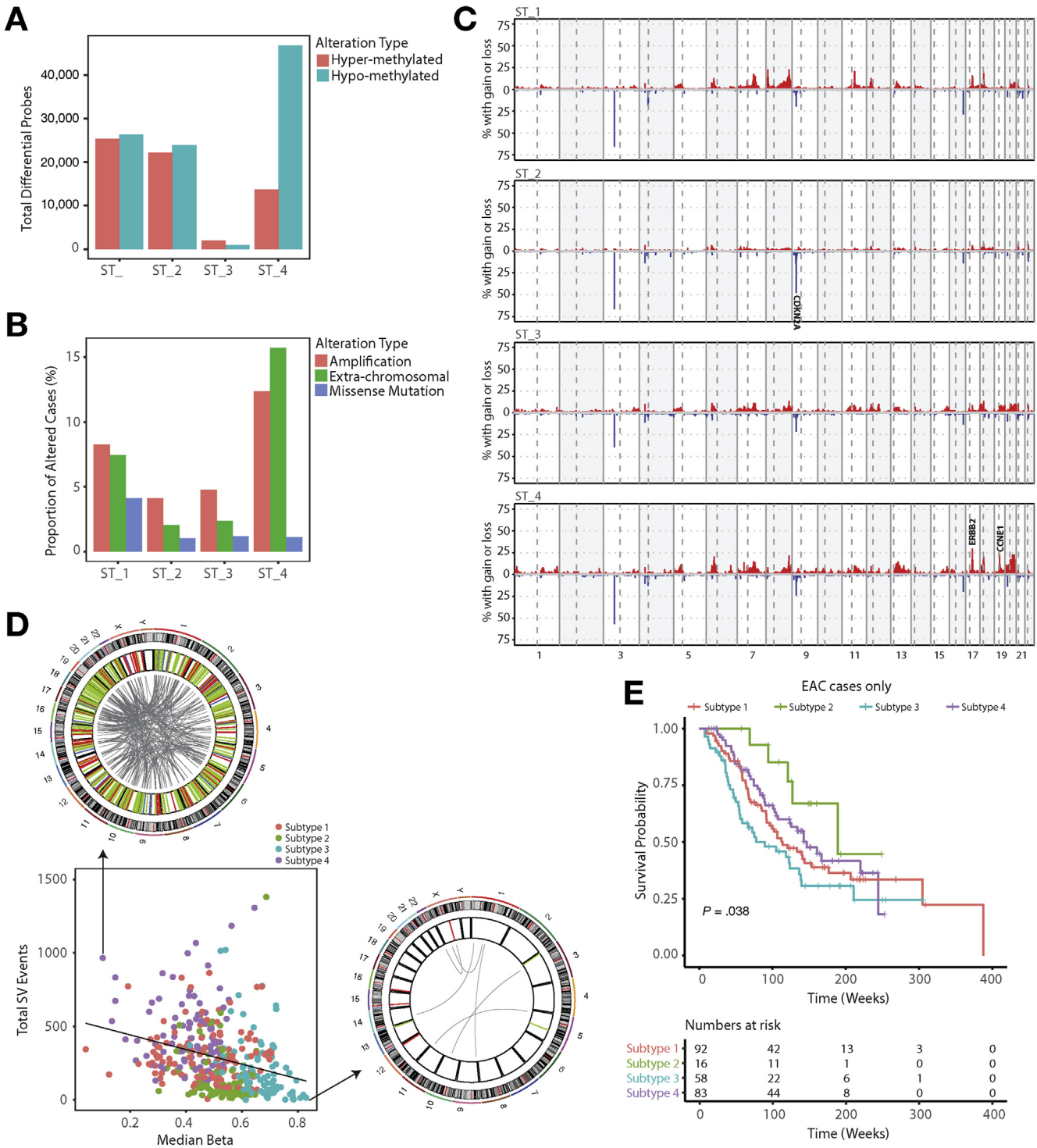

Figure 5. Hypomethylation-driven subtype 4. (*A*) Total number of hyper- and hypomethylation events observed across all 4 subtypes. (*B*) Genome-wide copy number alteration profile for all cases within individual subtype. (*C*) Proportion of cases harboring different forms of ERBB2 alternation across all 4 subtypes. (*D*) Correlation between SVs and median measure of methylation from probes undergoing hypomethylation from subtype 4 across all samples from different subtypes. Circos plot (on *top* and *right*) representing genome-wide SVs (deletions in *red*, duplication in *light green*, inversion in *blue*, and translocations in *gray*) from individual case undergoing high and low levels of hypomethylation. (*E*) Kaplan-Meier curves for EACs from 4 different subtypes.

unique pattern of methylation, mutation (Figure 1), and expression (Figure 2*D*, Supplementary Figure 5*A*–*C*). Furthermore, these subtypes were shown to be reproducible in an independent cohort from Australia,[11] even though the data had been generated on a different array platform.

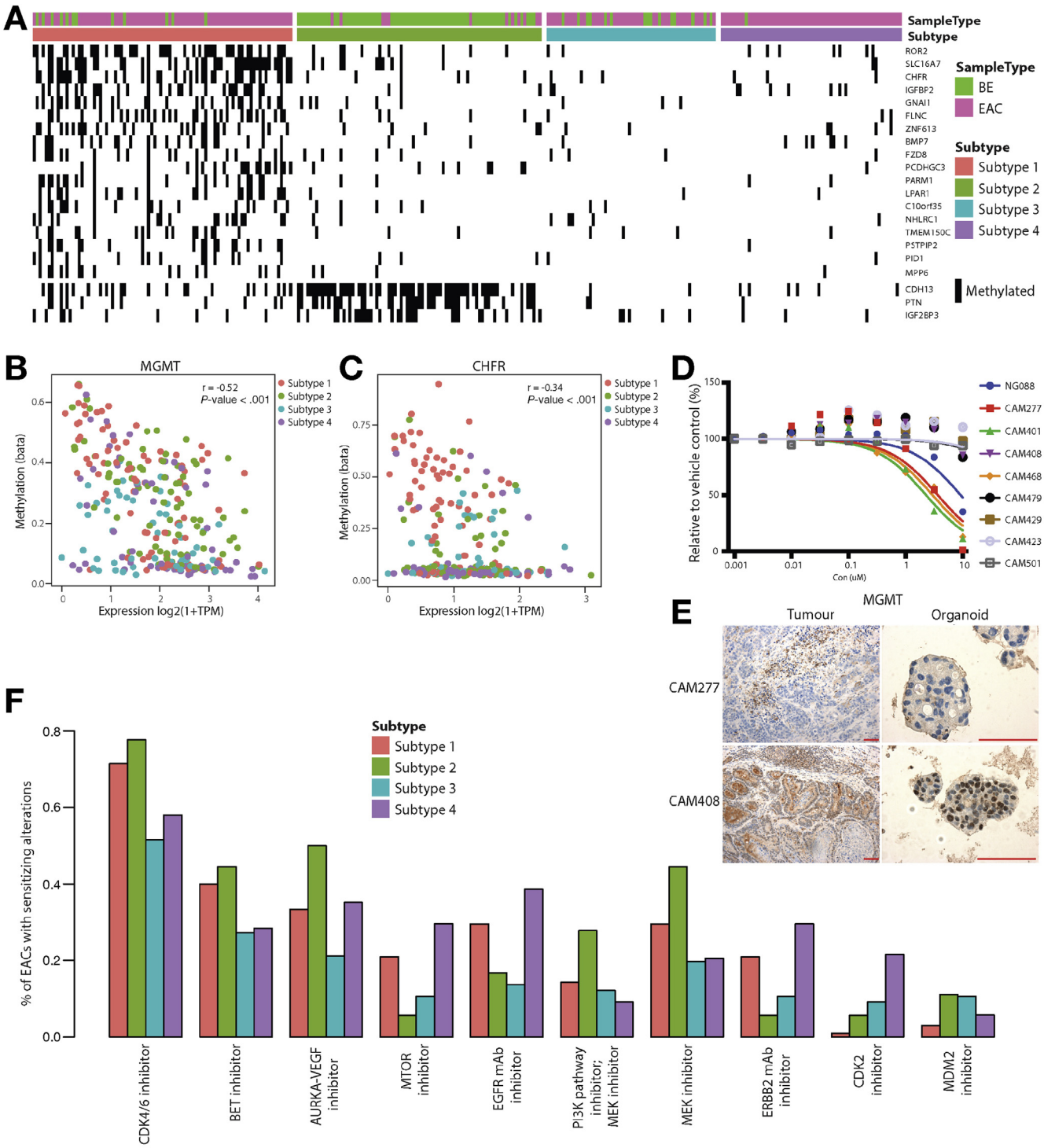

Figure 6. Epigenetically silenced genes and clinical relevance. (*A*) List of genes that are preferentially silenced either in subtype 1 or subtype 2. (*B*) Correlation between methylation and expression for MGMT gene across all cases from 4 different subtypes. (*C*) Same as (*B*) for CHFR gene. (*D*) Growth inhibition responses of 8 primary tumor–derived organoids and control gastric organoid (NG088) drug response to temozolomide. (*E*) MGMT staining in low (CAM277) and stable (CAM408)-expressing tumors and derived organoids (scale bar = 100 μM). (*F*) Drug classes for which sensitivity is indicated by EAC driver genes with data from the Cancer Biomarkers database.

Subtype 1 is dominated by EAC and some BE cases that show a gain in methylation in CpGi, which is representative of a CIMP-like phenotype, with preferential amplification for GATA4, CCND1, and signs of DNA repair. Subtype 2, with a preponderance of BE cases, also shows a gain in CpGi methylation like that of subtype 1 but with a unique pattern

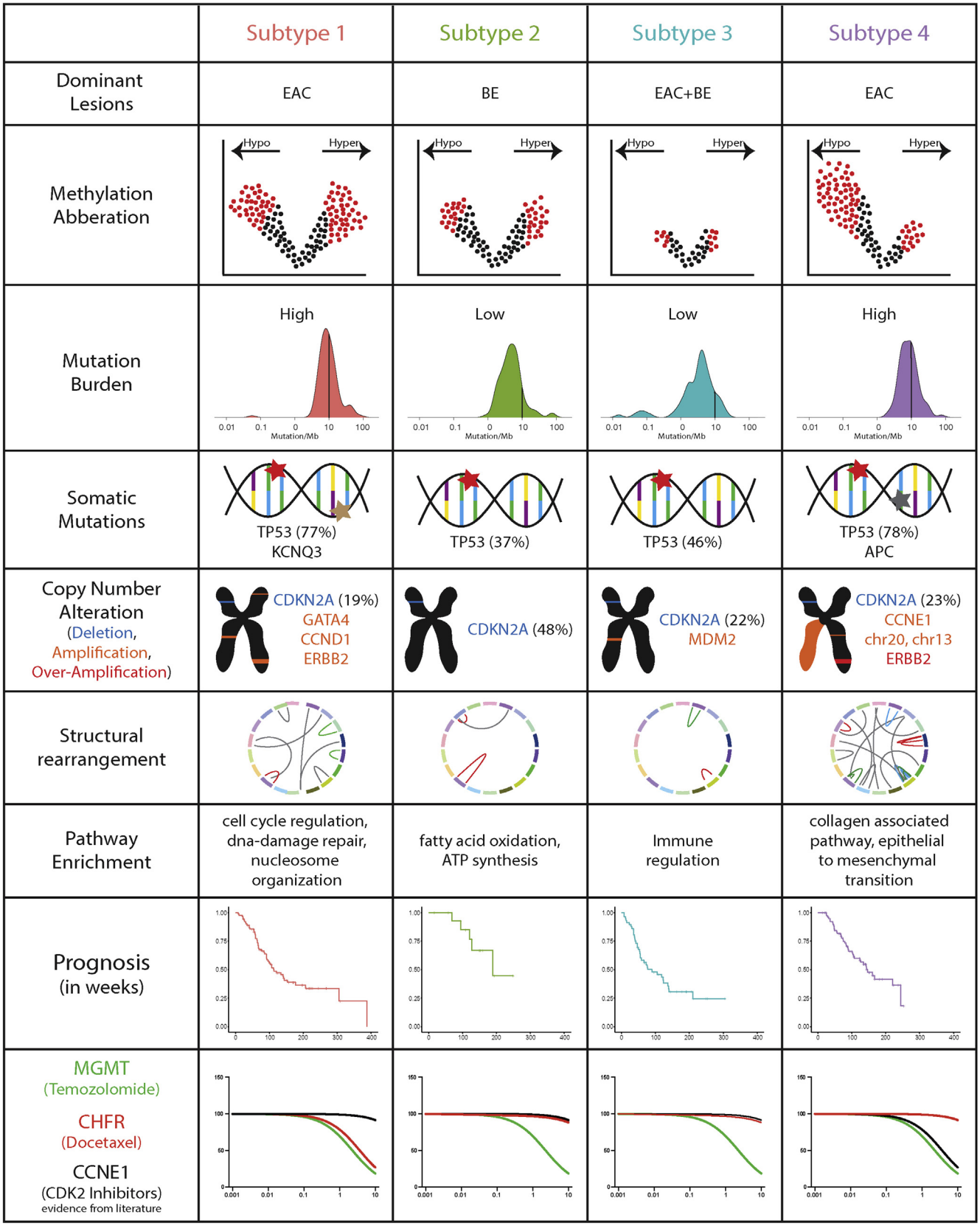

Figure 7. Overview of different biological features unique to individual subtypes.

of unmethylation. The transcriptomic profile of this subtype is uniquely enriched for ATP synthesis, fatty acid metabolism, and oxidation processes. Methylation levels in subtype 3 are unremarkable, but show a high-level presence of both myeloid and lymphoid cell lineages. Subtype 4 is characterized by hypomethylation and EAC cases harboring a high degree of genome stability supported by a high number of copy number alterations and SVs. Comprehensive molecular and biological features unique to each subtype identified through our analysis are presented in Figure 7.

We note that although most BE cases cluster together, they are somewhat distributed among subtypes 1 and 3 with the more stable genomes. Of 108 cases in subtype 1, 17 cases are BE and detailed inspection revealed that 15 of 17 cases were dysplastic with high-grade dysplasia or intramucosal carcinoma (Supplementary Figure 2*C*). On the other hand, some EAC cases (n = 20) cluster with the BE Subtype 2. Most of these tumors (11/20) have adjacent BE and are moderately differentiated (Supplementary Figure 2*A*), in keeping with better prognosis. This is in keeping with our previous observation that EAC with adjacent BE has a better prognosis.[51] In future, we would like to compare and study metabolic changes underlying such behavior.

In terms of prognosis, patients from subtype 3 with infiltration of immune-related cells tend to show a poor prognosis compared with patients in other subtypes. The tumor microenvironment is a complex network of interactions among tumor cells, immune cells, and stromal cells. Depending on their composition, different immune infiltrates are associated with good or poor prognosis. In general, tumor-infiltrating lymphocytes comprising cytotoxic CD8 T cells, memory T cells and T-helper cells are associated with a good prognosis, as is evident in many cancer types, such as breast,[52] ovary,[53] and lung,[54] whereas regulatory T cells, stromal cells, and immune cells of myeloid lineages (such as macrophages, neutrophils, mast cells, and others) are indicators of poor prognosis and can promote tumor progression.[55,56] In subtype 3, along with cytotoxic cells, we also notice a strong presence of macrophages, neutrophils, and CAFs, which could perhaps explain the poor prognosis of cases in this subtype. It is also worth noting that subtype 3 has a high prevalence of MDM2 amplification (8%), which is associated with resistance to and hyperprogression on immunotherapy.[57]

A recent study in EAC has shown that topoisomerase I inhibitors are effective in tumors with high levels of methylation.[12] Irinotecan is a topoisomerase I inhibitor chemotherapy that is currently used in EAC; however, irinotecan treatment has a low monotherapy response rate (~7%). This low response rate could potentially be enhanced if therapy is targeted to methylated tumors. As the TCGA demonstrates EAC to be very similar to CIN gastric cancer, we propose that subtype 1 representative of CIMP could possibly be sensitive to DNA methyltransferase and topoisomerase I inhibitors.

Through our integrated data analysis approach, we have shown how different genes from critical pathways are altered in EAC/BE. We also provide in vitro evidence from organoid models showing how key regulators of DNA repair (MGMT) and cell cycle (CHFR) can be targeted for effective treatment. In an extension of our previous work,[7] here we have shown other potential inhibitors like CDK2 could be preferentially effective toward subtype 4 cases. Taking all this information together, these results provide wider scope for better stratification and assignment of relevant targeted therapeutics.

It is also worth noting that all observations made in this study are derived from only the CpG sites present on the EPIC array. This is a narrow representation of the whole genome, and may be a limiting factor, as we cannot draw conclusions or understand changes in other parts of the genome and their influence in tumorigenesis. In future, it would be worth studying methylation on a genome-wide scale, perhaps though whole-genome bisulfite sequencing approaches.

In summary, this study elucidates diversity in the methylation landscape across BE and EAC and its influence on gene expression and genome integrity, suggesting a role for DNA methylation alteration in EAC carcinogenesis.

Supplementary Material

Note: To access the supplementary material accompanying this article, visit the online version of *Gastroenterology* at www.gastrojournal.org, and at https://doi.org/10.1053/j.gastro.2020.01.044.

References

1. Ferlay J, Soerjomataram I, Dikshit R, et al. Cancer incidence and mortality worldwide: sources, methods and major patterns in GLOBOCAN 2012. Int J Cancer 2015; 136:E359–E386.
2. Coleman HG, Xie SH, Lagergren J. The epidemiology of esophageal adenocarcinoma. Gastroenterology 2018; 154:390–405.
3. Smyth EC, Lagergren J, Fitzgerald RC, et al. Oesophageal cancer. Nat Rev Dis Primers 2017;3:17048.
4. Fitzgerald RC. Molecular basis of Barrett's oesophagus and oesophageal adenocarcinoma. Gut 2006;55:1810–1820.
5. Ross-Innes CS, Becq J, Warren A, et al. Whole-genome sequencing provides new insights into the clonal architecture of Barrett's esophagus and esophageal adenocarcinoma. Nat Genet 2015;47:1038–1046.
6. Secrier M, Li X, de Silva N, et al. Mutational signatures in esophageal adenocarcinoma define etiologically distinct subgroups with therapeutic relevance. Nat Genet 2016; 48:1131–1141.
7. Frankell AM, Jammula S, Li X, et al. The landscape of selection in 551 esophageal adenocarcinomas defines genomic biomarkers for the clinic. Nat Genet 2019; 51:506–516.
8. Stachler MD, Taylor-Weiner A, Peng S, et al. Paired exome analysis of Barrett's esophagus and adenocarcinoma. Nat Genet 2015;47:1047–1055.

9. Robertson KD. DNA methylation and chromatin—unraveling the tangled web. Oncogene 2002;21:5361–5379.
10. Jones PA, Baylin SB. The fundamental role of epigenetic events in cancer. Nat Rev Genet 2002;3:415–428.
11. Krause L, Nones K, Loffler KA, et al. Identification of the CIMP-like subtype and aberrant methylation of members of the chromosomal segregation and spindle assembly pathways in esophageal adenocarcinoma. Carcinogenesis 2016;37:356–365.
12. Yu M, Maden SK, Stachler M, et al. Subtypes of Barrett's oesophagus and oesophageal adenocarcinoma based on genome-wide methylation analysis [published online ahead of print June 8, 2018]. Gut doi: 10.1136/gutjnl-2017-314544.
13. Cancer Genome Atlas Research Network, Analysis Working Group: Asan University, BC Cancer Agency, et al. Integrated genomic characterization of oesophageal carcinoma. Nature 2017;541:169–175.
14. Fortin JP, Triche TJ Jr, Hansen KD. Preprocessing, normalization and integration of the Illumina HumanMethylationEPIC array with minfi. Bioinformatics 2017;33:558–560.
15. Teschendorff AE, Marabita F, Lechner M, et al. A beta-mixture quantile normalization method for correcting probe design bias in Illumina Infinium 450 k DNA methylation data. Bioinformatics 2013;29:189–196.
16. Tian Y, Morris TJ, Webster AP, et al. ChAMP: updated methylation analysis pipeline for Illumina BeadChips. Bioinformatics 2017;33:3982–3984.
17. Ritchie ME, Phipson B, Wu D, et al. limma powers differential expression analyses for RNA-sequencing and microarray studies. Nucleic Acids Res 2015;43:e47.
18. Brunet JP, Tamayo P, Golub TR, et al. Metagenes and molecular pattern discovery using matrix factorization. Proc Natl Acad Sci U S A 2004;101:4164–4169.
19. Jaffe AE, Murakami P, Lee H, et al. Bump hunting to identify differentially methylated regions in epigenetic epidemiology studies. Int J Epidemiol 2012;41:200–209.
20. Saunders CT, Wong WS, Swamy S, et al. Strelka: accurate somatic small-variant calling from sequenced tumor-normal sample pairs. Bioinformatics 2012;28:1811–1817.
21. Van Loo P, Nordgard SH, Lingjaerde OC, et al. Allele-specific copy number analysis of tumors. Proc Natl Acad Sci U S A 2010;107:16910–16915.
22. Chen X, Schulz-Trieglaff O, Shaw R, et al. Manta: rapid detection of structural variants and indels for germline and cancer sequencing applications. Bioinformatics 2016;32:1220–1222.
23. Lee AY, Ewing AD, Ellrott K, et al. Combining accurate tumor genome simulation with crowdsourcing to benchmark somatic structural variant detection. Genome Biol 2018;19:188.
24. Dobin A, Davis CA, Schlesinger F, et al. STAR: ultrafast universal RNA-seq aligner. Bioinformatics 2013;29:15–21.
25. Lawrence M, Huber W, Pages H, et al. Software for computing and annotating genomic ranges. PLoS Comput Biol 2013;9:e1003118.
26. Leek JT, Johnson WE, Parker HS, et al. The sva package for removing batch effects and other unwanted variation in high-throughput experiments. Bioinformatics 2012;28:882–883.
27. Robinson MD, McCarthy DJ, Smyth GK. edgeR: a Bioconductor package for differential expression analysis of digital gene expression data. Bioinformatics 2010;26:139–140.
28. Subramanian A, Tamayo P, Mootha VK, et al. Gene set enrichment analysis: a knowledge-based approach for interpreting genome-wide expression profiles. Proc Natl Acad Sci U S A 2005;102:15545–15550.
29. Hanzelmann S, Castelo R, Guinney J. GSVA: gene set variation analysis for microarray and RNA-seq data. BMC Bioinformatics 2013;14:7.
30. Tamborero D, Rubio-Perez C, Muinos F, et al. A pan-cancer landscape of interactions between solid tumors and infiltrating immune cell populations. Clin Cancer Res 2018;24:3717–3728.
31. Zheng S, Cherniack AD, Dewal N, et al. Comprehensive pan-genomic characterization of adrenocortical carcinoma. Cancer Cell 2016;29:723–736.
32. Silva TC, Coetzee SG, Gull N, et al. ELMER v.2: an R/Bioconductor package to reconstruct gene regulatory networks from DNA methylation and transcriptome profiles. Bioinformatics 2019;35:1974–1977.
33. Pidsley R, Zotenko E, Peters TJ, et al. Critical evaluation of the Illumina MethylationEPIC BeadChip microarray for whole-genome DNA methylation profiling. Genome Biol 2016;17:208.
34. Consortium EP. An integrated encyclopedia of DNA elements in the human genome. Nature 2012;489:57–74.
35. Davis CA, Hitz BC, Sloan CA, et al. The Encyclopedia of DNA elements (ENCODE): data portal update. Nucleic Acids Res 2018;46:D794–D801.
36. Roadmap Epigenomics Consortium, Kundaje A, Meuleman W, et al. Integrative analysis of 111 reference human epigenomes. Nature 2015;518:317–330.
37. Chen L, Huang M, Plummer J, et al. Master transcription factors form interconnected circuitry and orchestrate transcriptional networks in oesophageal adenocarcinoma [published online ahead of print August 13, 2019]. Gut doi: 10.1136/gutjnl-2019-318325.
38. Xie JJ, Jiang YY, Jiang Y, et al. Super-enhancer-driven long non-coding RNA LINC01503, regulated by TP63, is over-expressed and oncogenic in squamous cell carcinoma. Gastroenterology 2018;154:2137–2151.e1.
39. Sheaffer KL, Elliott EN, Kaestner KH. DNA hypomethylation contributes to genomic instability and intestinal cancer initiation. Cancer Prev Res (Phila) 2016;9:534–546.
40. Cheng P, Schmutte C, Cofer KF, et al. Alterations in DNA methylation are early, but not initial, events in ovarian tumorigenesis. Br J Cancer 1997;75:396–402.
41. Bedford MT, van Helden PD. Hypomethylation of DNA in pathological conditions of the human prostate. Cancer Res 1987;47:5274–5276.
42. Kim YI, Giuliano A, Hatch KD, et al. Global DNA hypomethylation increases progressively in cervical dysplasia and carcinoma. Cancer 1994;74:893–899.

43. Feinberg AP, Gehrke CW, Kuo KC, et al. Reduced genomic 5-methylcytosine content in human colonic neoplasia. Cancer Res 1988;48:1159–1161.
44. Ehrlich M, Jiang G, Fiala E, et al. Hypomethylation and hypermethylation of DNA in Wilms tumors. Oncogene 2002;21:6694–6702.
45. Alvarez H, Opalinska J, Zhou L, et al. Widespread hypomethylation occurs early and synergizes with gene amplification during esophageal carcinogenesis. PLoS Genet 2011;7:e1001356.
46. Wu W, Bhagat TD, Yang X, et al. Hypomethylation of noncoding DNA regions and overexpression of the long noncoding RNA, AFAP1-AS1, in Barrett's esophagus and esophageal adenocarcinoma. Gastroenterology 2013;144:956–966.e4.
47. Liu X, Cheng Y, Abraham JM, et al. Modeling Wnt signaling by CRISPR-Cas9 genome editing recapitulates neoplasia in human Barrett epithelial organoids. Cancer Lett 2018;436:109–118.
48. Li X, Francies HE, Secrier M, et al. Organoid cultures recapitulate esophageal adenocarcinoma heterogeneity providing a model for clonality studies and precision therapeutics. Nat Commun 2018;9:2983.
49. Hegi ME, Diserens AC, Gorlia T, et al. MGMT gene silencing and benefit from temozolomide in glioblastoma. N Engl J Med 2005;352:997–1003.
50. Yun T, Liu Y, Gao D, et al. Methylation of CHFR sensitizes esophageal squamous cell cancer to docetaxel and paclitaxel. Genes Cancer 2015;6:38–48.
51. Sawas T, Killcoyne S, Iyer PG, et al. Identification of prognostic phenotypes of esophageal adenocarcinoma in 2 independent cohorts. Gastroenterology 2018;155:1720–1728.e4.
52. Jeschke J, Bizet M, Desmedt C, et al. DNA methylation-based immune response signature improves patient diagnosis in multiple cancers. J Clin Invest 2017;127:3090–3102.
53. Leffers N, Gooden MJ, de Jong RA, et al. Prognostic significance of tumor-infiltrating T-lymphocytes in primary and metastatic lesions of advanced stage ovarian cancer. Cancer Immunol Immunother 2009;58:449–459.
54. Ruffini E, Asioli S, Filosso PL, et al. Clinical significance of tumor-infiltrating lymphocytes in lung neoplasms. Ann Thorac Surg 2009;87:365–371; discussion 371–372.
55. Fridman WH, Pages F, Sautes-Fridman C, et al. The immune contexture in human tumours: impact on clinical outcome. Nat Rev Cancer 2012;12:298–306.
56. Barnes TA, Amir E. HYPE or HOPE: the prognostic value of infiltrating immune cells in cancer. Br J Cancer 2017;117:451–460.
57. Kato S, Goodman A, Walavalkar V, et al. Hyperprogressors after immunotherapy: analysis of genomic alterations associated with accelerated growth rate. Clin Cancer Res 2017;23:4242–4250.

Received September 12, 2019. Accepted January 29, 2020.

Correspondence
Address correspondence to: Rebecca C. Fitzgerald, MD, MRC Cancer Unit, Hutchison/MRC Research Centre, University of Cambridge, Box 197, Cambridge Biomedical Campus, Cambridge, UK CB2 0XZ. e-mail: rcf29@MRC-CU.cam.ac.uk.

Acknowledgments

Oesophageal Cancer Clinical and Molecular Stratification (OCCAMS) Consortium:

Rebecca C. Fitzgerald[1], Ayesha Noorani[1], Paul A.W. Edwards[1,2], Nicola Grehan[1], Barbara Nutzinger[1], Caitriona Hughes[1], Elwira Fidziukiewicz[1], Jan Bornschein[1], Shona MacRae[1],Jason Crawte[1], Alex Northrop[1], Gianmarco Contino[1], Xiaodun Li[1],Rachel de la Rue[1], Maria O'Donovan[1,3], Ahmad Miremadi[1,3], Shalini Malhotra[1,3], Monika Tripathi[1,3], Simon Tavaré[2], Andy G. Lynch[2], Matthew Eldridge[2], Maria Secrier[2], Lawrence Bower[2], Ginny Devonshire[2], Juliane Perner[2], Sriganesh Jammula[2], Jim Davies[5], Charles Crichton[5], Nick Carroll[6], Peter Safranek[6], Andrew Hindmarsh[6], Vijayendran Sujendran[6], Stephen J. Hayes[7,14], Yeng Ang[7,8,29], Shaun R. Preston[9], Sarah Oakes[9], Izhar Bagwan[9], Vicki Save[10], Richard J.E. Skipworth[10], Ted R. Hupp[10], J. Robert O'Neill[10,23], Olga Tucker[11,33], Andrew Beggs[11,28], Philippe Taniere[11], Sonia Puig[11],Timothy J. Underwood[12,13], Fergus Noble[12], Jack Owsley[12], Hugh Barr[15], Neil Shepherd[15], Oliver Old[15], Jesper Lagergren[16,25], James Gossage[16,24], Andrew Davies[16,24],Fuju Chang[16,24],Janine Zylstra[16,24], Ula Mahadeva[18], Vicky Goh[24], Francesca D. Ciccarelli[24], Grant Sanders[17], Richard Berrisford[17], Catherine Harden[17], Mike Lewis[18], Ed Cheong[18], Bhaskar Kumar[18],Simon L Parsons[19], Irshad Soomro[19], Philip Kaye[19], John Saunders[19], Laurence Lovat[20], Rehan Haidry[20], Laszlo Igali[21], Michael Scott[22], Sharmila Sothi[26], Sari Suortamo[26], Suzy Lishman[27], George B. Hanna[31], Krishna Moorthy[31], Christopher J. Peters[31], Anna Grabowska[32], Richard Turkington[34].

[1] Medical Research Council Cancer Unit, Hutchison/Medical Research Council Research Centre, University of Cambridge, Cambridge, UK; [2]Cancer Research UK Cambridge Institute, University of Cambridge, Cambridge, UK; [3]Department of Histopathology, Addenbrooke's Hospital, Cambridge, UK; [4]Oxford ComLab, University of Oxford, UK, OX1 2JD;[5]Department of Computer Science, University of Oxford, UK, OX1 3QD; [6]Cambridge University Hospitals NHS Foundation Trust, Cambridge, UK, CB2 0QQ; [7]Salford Royal NHS Foundation Trust, Salford, UK, M6 8HD; [8]Wigan and Leigh NHS Foundation Trust, Wigan, Manchester, UK, WN1 2NN; [9]Royal Surrey County Hospital NHS Foundation Trust, Guildford, UK, GU2 7XX; [10]Edinburgh Royal Infirmary, Edinburgh, UK, EH16 4SA;[11]University Hospitals Birmingham NHS Foundation Trust, Birmingham, UK, B15 2GW;[12]University Hospital Southampton NHS Foundation Trust, Southampton, UK, SO16 6YD;[13]Cancer Sciences Division, University of Southampton, Southampton, UK, SO17 1BJ;[14]Faculty of Medical and Human Sciences, University of Manchester, UK, M13 9PL; [15]Gloucester Royal Hospital, Gloucester, UK, GL1 3NN; [16]Guy's and St Thomas's NHS Foundation Trust, London, UK, SE1 7EH; [17]Plymouth Hospitals NHS Trust, Plymouth, UK, PL6 8DH; [18]Norfolk and Norwich University Hospital NHS Foundation Trust, Norwich, UK, NR4 7UY; [19]Nottingham University Hospitals NHS Trust, Nottingham, UK, NG7 2UH; [20]University College London, London, UK, WC1E 6BT; [21]Norfolk and Waveney Cellular Pathology Network, Norwich, UK, NR4 7UY; [22]Wythenshawe Hospital, Manchester, UK, M23 9LT;[23]Edinburgh University, Edinburgh, UK, EH8 9YL; [24]King's College London, London, UK, WC2R 2LS; [25]Karolinska Institutet, Stockholm, Sweden, SE-171 77; [26]University Hospitals Coventry and Warwickshire NHS, Trust, Coventry, UK, CV2 2DX; [27]Peterborough Hospitals NHS Trust, Peterborough City Hospital, Peterborough, UK, PE3 9GZ; [28]Institute of Cancer and Genomic sciences, University of Birmingham, B15 2TT; [29]GI science centre, University of Manchester, UK, M13 9PL; [30]Queen's Medical Centre, University of Nottingham, Nottingham, UK, NG7 2UH; [31]Department of Surgery and Cancer, Imperial College London, UK, W2 1NY; [32]Queen's Medical Centre, University of Nottingham, Nottingham, UK; [33]Heart of England NHS Foundation Trust, Birmingham, UK, B9 5SS; [34]Centre for Cancer Research and Cell Biology, Queen's University Belfast, Northern Ireland, UK, BT7 1NN.

OCCAMS was funded by a Programme Grant from Cancer Research UK (RG81771/84119), and the laboratory of RCF is funded by a Core Programme Grant from the Medical Research Council (RG84369). We thank the Human Research Tissue Bank, which is supported by the UK National Institute for Health Research (NIHR) Cambridge Biomedical Research Centre, from Addenbrooke's Hospital. Additional infrastructure support was provided from the Cancer Research UK–funded Experimental Cancer Medicine Centre.

We acknowledge Dr Andrew Beggs and Dr Celina Whalley from the Institute of Cancer and Genomic Sciences, University of Birmingham, who provided services for profiling methylation on all our samples.

Vinod V. Subash's current address: Children's Cancer Institute Australia, Lowy Cancer Research Centre, UNSW Sydney, Kensington, NSW 2052, Australia

CRediT Authorship Contributions

Sriganesh Jammula, PhD (Conceptualization: Lead; Data curation: Lead; Formal analysis: Lead; Investigation: Lead; Methodology: Lead; Project administration: Lead;

Software: Lead; Validation: Lead; Visualization: Lead; Writing – original draft: Lead;

Writing – review & editing: Lead). Annalise C. Katz-Summercorn, MA MBBChir (Data curation: Equal; Resources: Equal; Writing – review & editing: Supporting). Xiaodun Li, PhD (Validation: Equal; Writing – review & editing:

Supporting). Constanza Linossi, MD (Validation: Supporting; Visualization: Supporting; Writing –review & editing: Supporting)

Elizabeth Smyth, MD (Writing – review & editing: Supporting). Sarah Killcoyne, PhD (Resources: Supporting; Writing – review & editing: Supporting). Daniele Biasci, PhD (Resources: Supporting; Writing – review & editing: Supporting). Vinod V. Subash, PhD (Resources: Supporting; Writing – review & editing: Supporting). Sujath Abbas, MSc (Resources: Supporting; Writing – review & editing: Supporting). Adrienn Blasko, BSc (Resources: Supporting; Writing – review & editing: Supporting). Ginny Devonshire, MSc (Resources: Supporting; Writing – review & editing: Supporting). Amber Grantham, PhD (Resources: Supporting; Writing – review & editing: Supporting). Filip Wronowski, BS (Resources: Supporting; Writing – review & editing: Supporting). Maria O'Donovan, MB, MD, FRCPath (Resources: Supporting; Writing – review & editing: Supporting). Nicola Grehan, RGN,RMN (Resources: Supporting; Writing – review & editing: Supporting).

Matthew Eldridge, PhD (Resources: Supporting; Writing – review & editing: Supporting).

Simon Tavaré, PhD (Supervision: Supporting; Writing – review & editing: Supporting).

Rebecca C Fitzgerald, MD (Conceptualization: Lead; Funding acquisition: Lead;

Supervision: Lead; Writing – review & editing: Supporting).

Conflicts of interest

The authors disclose no conflicts. Simon Tavaré is a consultant for Kallyope Inc. and is a member of the SAB of Ipsen. These are not directly involved in the topic of this paper. Rebecca Fitzgerald is named on patents related to Cytosponge and related assays which have been licensed by the Medical Research Council to Covidien GI Solutions (now Medtronic).

Funding

OCCAMS was funded by a Programme Grant from Cancer Research UK (RG81771/84119), and the laboratory of Rebecca C. Fitzgerald is funded by a Core Programme Grant from the Medical Research Council (RG84369).

Supplementary Methods

Gene Expression Profiling

Total RNA was extracted using All Prep DNA/RNA kit from Qiagen and the quality was checked on an Agilent 2100 Bioanalyzer using the RNA 6000 nano kit (Agilent). The Qubit high sensitivity RNA assay kit from Thermo Fisher was used for quantification. Libraries were prepared from 250ng RNA, using TruSeq Stranded Total RNA Library Prep Gold (Ribo-zero) kit and ribosomal RNA (nuclear, cytoplasmic and mitochondrial rRNA) was depleted, whereby biotinylated probes selectively bind to ribosomal RNA molecules forming probe-rRNA hybrids. These hybrids were pulled down using magnetic beads and rRNA depleted total RNA was reverse transcribed. The libraries were prepared according to the Illumina protocol.[1] Paired-end 75bp sequencing on HiSeq4000 generated the paired end reads.

Histone Modification Profiling

We downloaded ChIP-seq data for H3K27me3 and H3K27ac histone modifications in aligned form for esophagus, gastric and duodenum tissues from ENCODE[2,3]/ROADMAP[4] consortium data portal. We quantified two histone modifications across all normal tissues on extended regions (5kb both up and downstream from centre) that were gaining methylation in Subtype I as compared to controls. The quantification shown in Figure 2 was generated using ngs.plot.[5]

Organoid culture and Drug treatment

The primary organoid cultures were derived from one normal gastric case and eight EAC cases included in the OCCAMS/ICGC sequencing study. Detailed organoid culture and derivation method have been previously described.[6] Regarding the drug treatment, the seeding density for each line was optimised to ensure cell growth in the logarithmic growth phase. Cells were seeded in complete medium for 24 hours then treated with compounds at a 9-point half-log serial dilutions for 6 days. Cell viability was assessed using CellTiter-Glo (Promega) after drug incubation. The concentrations of a compound causing 50% growth inhibition relative to the vehicle control (GI50) were determined by nonlinear regression dose-response analysis and the area under the curve (AUC) was calculated using GraphPad Prism.

Granzyme B (GZMB) Immunohistochemistry

FFPE tissues are sectioned at 4um thickness, floated onto charged glass slides and dried at 37oC overnight. Deparaffinisation (69°C for 32min), antigen retrieval (pH8 with CC1), peroxidase inhibition (Discovery inhibitor/inhibitor CM) and indirect IHC are conducted with the automated Ventana Discovery Ultra platform and Leica Bond. Primary antibody for Granzyme B from Abcam (EPR8260) was used in this study.

Performance of primary antibodies is compared against negative isotype controls. Mouse monoclonal antibodies are ready-to-use (RTU) preparations manufactured by Roche. Rabbit primary Ab negative control is produced by DAKO at a concentration of 1500 uL/mL. This negative isotype is diluted to match the concentration of the tested primary antibody. For counterstaining and post-counterstaining, haematoxylin and bluing reagent are consecutively applied to the sections, and each is incubated for 16 minutes. Slides are washed with reaction buffer after each incubation, throughout the automated process.

Stained slides are dehydrated and automatically coverslipped using the Leica Autostainer ST020. They are digitally scanned by Aperio Scanscope XT at a 20X resolution. Images are annotated digitally using the HALO® TM digital image analysis software v2.1.1637.11 (Indica Labs, Corrales, NM). In total, IHC data for GZMB was available for 17 EAC cases.

MGMT Immunohistochemistry

Paraffin embedded sections of 3.5 μm were used for immunohistochemistry by a Bond Max autostainer according to the manufacturer's instruction (Leica Microsystems). Primary antibodies MGMT (MT3.1, Merck, 1:100 dilution) were optimized (incubation 30 mins) and applied with controls.

Pathway Analysis

Gene Ontology and Pathway analysis of silenced gene was performed using David[7] and IPA (QIAGEN Inc., https://www.qiagenbioinformatics.com/products/ingenuitypathway-analysis).

References

1. Nagai K, Kohno K, Chiba M, et al. Differential expression profiles of sense and antisense transcripts between HCV-associated hepatocellular carcinoma and corresponding non-cancerous liver tissue. Int J Oncol 2012; 40:1813–1820.
2. Consortium EP. An integrated encyclopedia of DNA elements in the human genome. Nature 2012;489:57–74.
3. Davis CA, Hitz BC, Sloan CA, et al. The Encyclopedia of DNA elements (ENCODE): data portal update. Nucleic Acids Res 2018;46:D794–D801.
4. Roadmap Epigenomics C, Kundaje A, Meuleman W, et al. Integrative analysis of 111 reference human epigenomes. Nature 2015;518:317–330.
5. Shen L, Shao N, Liu X, et al. ngs.plot: Quick mining and visualization of next-generation sequencing data by integrating genomic databases. BMC Genomics 2014; 15:284.
6. Li X, Francies HE, Secrier M, et al. Organoid cultures recapitulate esophageal adenocarcinoma heterogeneity providing a model for clonality studies and precision therapeutics. Nat Commun 2018;9:2983.
7. Huang da W, Sherman BT, Lempicki RA. Systematic and integrative analysis of large gene lists using DAVID bioinformatics resources. Nat Protoc 2009;4:44–57.